

# Structure–Property Relationships of Cellulose Nanocrystals and Nanofibrils: Implications for the Design and Performance of Nanocomposites and All-Nanocellulose Systems

Camilla H. M. Camargos and Camila A. Rezende\*

Cite This: *ACS Appl. Nano Mater.* 2021, 4, 10505–10518

Read Online

ACCESS |



Metrics &amp; More



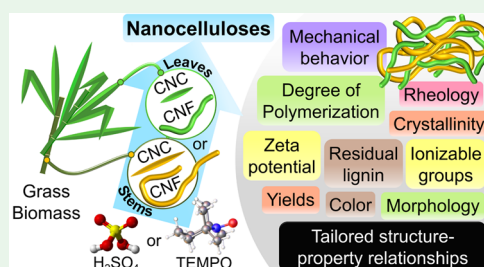
Article Recommendations



Supporting Information

**ABSTRACT:** Cellulose nanocrystals (CNCs) and nanofibrils (CNFs) are sustainable candidates for designing nanocomposites and all-nanocellulose systems for a myriad of advanced applications, such as protective coatings, packaging materials, and hydrogels. The role of nanocellulose in such different applications is mainly determined by its morphological and physicochemical properties. Although these properties have been studied at length by a consistent and growing number of publications, there is still a lack of a comprehensive study of the relationships between structure, properties, and functions of different nanocelluloses. Here, we thoroughly investigated the combined effect of distinct production methods and anatomical origins of non-wood cellulose on the structure–property relationships of CNCs and CNFs. These nanoparticles were obtained by the most established production approaches, that is, sulfuric acid hydrolysis or TEMPO-mediated oxidation/fibrillation of elephant grass leaves or stems, that is, two different parts of a unique biosource. We were able to prepare CNCs and CNFs with modulated morphological features and degrees of polymerization, which implied major effects on the mechanical and rheological behaviors of nanocellulose films and dispersions, respectively. Additionally, tailoring lignin and ionizable group contents as well as the color, transparency, and stability of nanocellulose dispersions could provide important implications for the shelf life of nanocellulose formulations, as well as for their application as nanocomposite additives with UV-protection and antioxidant abilities. Therefore, the assembly of results presented here can work as a tool to guide decision-making for both (1) the selection of methods and/or plant anatomical parts to produce nanocelluloses with tailored properties and (2) the prospects of combining different cellulose nanostructures to design advanced materials.

**KEYWORDS:** nanocellulose, lignin-containing nanocellulose, nanocomposite, elephant grass, acid hydrolysis, TEMPO-oxidation, sonication



## INTRODUCTION

Cellulose nanocrystals (CNCs) and nanofibrils (CNFs) extracted from lignocellulosic biomasses gather industrial and scientific relevance due to their high amenability for surface-functionalization, flexibility, durability, uniformity, and great mechanical strength performance.<sup>1</sup> These enhanced properties are intrinsically related to cell wall and cellulose biosyntheses. The multistep biosynthetic process dictates the crystallinity, aspect ratio, and morphology of cellulose microfibrils, which are then expected to alter the characteristics of the produced nanocelluloses and their role in different applications.<sup>2,3</sup>

While both CNCs and CNFs have diameters in the range of 3–20 nm, CNCs have an average length of 50–500 nm, presenting needle-shaped morphology, with an aspect ratio usually between ~5 and 50, high crystallinity, and rigid structure. CNFs, on the other hand, are elongated fibrils with an average length between 500 nm and 2 μm. Therefore, they usually have an aspect ratio higher than 100 and are flexible nanostructures, containing both amorphous and crystalline domains.<sup>2,4</sup>

Nanocrystals and nanofibrils can be prepared by chemical, mechanical, or chemomechanical processes. Acid hydrolysis,

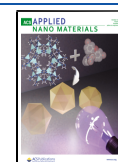
the most conventional method to produce CNCs,<sup>3</sup> comprises the preferential cleavage and degradation of the amorphous regions of cellulose chains.<sup>5</sup> The canonical process by sulfuric acid hydrolysis introduces sulfate half-ester groups onto the CNC surface.<sup>6</sup> Alternatively, hydrochloric acid,<sup>7</sup> hydrobromic acid,<sup>8</sup> formic acid,<sup>9</sup> phosphoric acid,<sup>10</sup> and mixtures of citric/hydrochloric acids<sup>11</sup> yield CNCs with different functionalities—from minimal surface charge with HCl, HBr, and CH<sub>2</sub>O<sub>2</sub>, to phosphate and carboxylate-rich surfaces using H<sub>3</sub>PO<sub>4</sub> or C<sub>6</sub>H<sub>8</sub>O<sub>7</sub>/HCl, respectively.

In contrast, TEMPO-mediated oxidation, followed by mechanical fibrillation has been introduced as an acid-free methodology to prepare CNCs<sup>12,13</sup> and is, in fact, the current trend to produce CNFs. By oxidation, C6-primary hydroxyls

Received: July 19, 2021

Accepted: September 7, 2021

Published: September 21, 2021



are regioselectively converted into carboxylate groups, increasing electrostatic repulsion and favoring the fibrillation of cellulose during the subsequent mechanical step.<sup>4</sup> Alternatively, CNFs can also be obtained by successive cellulose refining, followed by enzymatic hydrolysis and mechanical fibrillation or homogenization,<sup>14</sup> by cellulose carboxymethylation<sup>15</sup> or quaternization,<sup>16</sup> followed by homogenization/microfluidization, and even by unusual methods, such as fibrillation induced by the crystallization of salts (sodium and magnesium sulfates) inside the cellulose fiber matrix.<sup>17</sup>

Regarding the two most commonly used methods to prepare CNCs and CNFs, namely, sulfuric acid hydrolysis and TEMPO-mediated oxidation, different properties of sulfated and carboxylated nanocelluloses have been previously compared. For instance, the presence of chirality as well as variation in particle surface chemistry, dimensions, and morphology were reported for wood versus bacterial CNCs.<sup>18</sup> Similar morphology was identified for sulfated and carboxylated CNCs extracted by acid hydrolysis from *Juncus* plant stems,<sup>11</sup> while CNCs and CNFs obtained, respectively, by sulfuric acid hydrolysis of microcrystalline cellulose and mechanical shearing of softwood pulp presented different particle lengths and rheological properties.<sup>19</sup> However, no comprehensive study has so far encompassed the simultaneous production and characterization of CNFs and CNCs using both the most established production methods on a single biomass resource.

Different production approaches result in different properties of paramount importance for the application of nanocelluloses, establishing a consistent structure–property–function relationship. For instance, characteristics such as length, aspect ratio, crystallinity, and degree of polymerization influence the optical transmittance, tensile strength, and oxygen-barrier properties of CNF films and coatings.<sup>20</sup> In turn, the CNC surface charge and zeta potential, as well as the presence of residual lignin in CNFs, affect the capacity of these nanostructures to stabilize Pickering emulsions.<sup>21,22</sup> Additionally, lignin-containing CNFs are outstanding nanocomposite nanofillers with UV-shielding,<sup>23</sup> antioxidant,<sup>24</sup> and viscosity-modulating properties.<sup>25,26</sup>

The present work reports the concomitant production of CNFs and CNCs from elephant grass (*Pennisetum purpureum*) using two pathways: sulfuric acid hydrolysis and TEMPO-oxidation, followed by sonication. This perennial forage crop, found as agricultural surplus or waste, contains a high concentration of cellulose (more than 30 wt %) in both leaves and stems,<sup>27</sup> which were separately converted into cellulose nanostructures. Thus, in addition to addressing the effect of production methods, this study also provided innovative insights into the role of plant anatomical origins in CNC and CNF features. Here, different nanoparticle characteristics were assessed via chemical and morphological analysis, as well as colloidal stability assays, rheological measurements, and mechanical tensile testing of nanocellulose films. Concurrently, the anatomical origins of cellulose and the different production methods influenced nanoparticle yields, lengths, degree of polymerization, and rheological behavior. In turn, the preparation method alone had a major contribution in determining the lignin and ionizable group contents, as well as the color and stability of nanocellulose dispersions. This systematic assembly of results sheds light on the contribution of the most established production methods and other

ancillary factors, such as anatomical origin, in tailoring crucial properties of nanocelluloses. Combining leaf and stem CNFs to produce thin films was proven to increase tensile strength and stiffness as compared to single-component films. Therefore, controlling nanocellulose structural features by implementing different production methods on different parts of lignocellulosic precursors could be a handy strategy for designing sustainable building blocks for a variety of applications, including nanocomposites,<sup>2,28</sup> all-nanocellulose thin films,<sup>29</sup> coatings,<sup>30</sup> lightweight 3D networks,<sup>31</sup> and other advanced materials.

## ■ EXPERIMENTAL SECTION

**Biomass Pretreatments and Chemical Composition.** Elephant grass, also known as Napier or Uganda grass, was kindly supplied by the Institute of Animal Science (Instituto de Zootecnia-SP, Nova Odessa, Brazil). Plants were harvested after one year of planting, separated into leaves and stems, oven dried at 60 °C for 24 h, and knife milled through a 10 mesh sieve. Then, the biomass underwent a sequential two-step acid–alkaline pretreatment with diluted H<sub>2</sub>SO<sub>4</sub> and NaOH by following previous reports<sup>32,33</sup> with minor modifications. This process was conducted to isolate a cellulose-enriched substrate prone to be converted into nanocelluloses. Extractives, ash, structural carbohydrates, soluble and insoluble lignin in untreated (*in natura*) and pretreated biomass were quantified according to standard protocols.<sup>34</sup> Refer to [Supporting Information](#) (SI) for the complete list of reactants and detailed pretreatment procedures and characterization of *in natura* and pretreated biomass (Table S1, Figures S1 and S2).

**Acid Hydrolysis.** The milled cellulose-enriched substrate from leaves or stems was hydrolyzed with 60 wt % H<sub>2</sub>SO<sub>4</sub> at 45 ± 5 °C under constant mechanical stirring for 40 min, according to a methodology previously described for elephant grass leaves<sup>32</sup> with modifications. Acid-hydrolyzed CNCs (AH-CNCs) and nanofibrils (AH-CNFs) were recovered in different fractions of a single production process consisting of multiple steps (hydrolysis, quenching with iced water, and successive centrifugation). Water-dispersed AH-CNCs were obtained from the hydrolysis of the supernatant after washing steps by centrifugation, while AH-CNFs were recovered as a slurry from the pellet remaining after centrifugation. The experimental details are provided in [Supporting Information](#).

**TEMPO-Mediated Oxidation, Followed by Sonication.** TEMPO-mediated oxidation of the milled cellulose-enriched substrate from leaves or stems was performed with adjustments to previous methodologies.<sup>12,13,35</sup> In brief, each gram of the substrate was oxidized in water with 60 mmol of NaClO, 0.1 mmol of TEMPO, and 1 mmol of NaBr. After homogenization, the conversion of oxidized cellulose into TEMPO-oxidized CNFs (TO-CNFs) was conducted via probe-sonication for 30 min. Dilution and further sonication for another 30 min yielded TEMPO-oxidized CNCs (TO-CNCs). The experimental details are provided in [Supporting Information](#).

**Nanocellulose Characterization: Morphology, Crystallinity, Degree of Polymerization, Lignin Content, Surface Chemistry, Colloidal Stability, and Rheological Properties.** The average diameter and length of CNCs and CNFs, as well as their particle morphology, were assessed by transmission electron (TEM) and atomic force (AFM) microscopies. The cellulose crystallinity index (CrI) was estimated using X-ray diffractometry (XRD) analysis.<sup>36</sup> The average degree of polymerization (DP<sub>n</sub>) was estimated by a viscosimetric method using bis(ethylenediamine)copper(II) hydroxide (CED) as solvent.<sup>37,38</sup> The content of residual lignin in nanocelluloses was determined using the acetyl bromide soluble lignin (ABSL) method.<sup>33</sup> Light transmittance spectra of nanocellulose aqueous dispersions were assessed by ultraviolet–visible (UV–Vis) spectroscopy. Ionizable groups on the CNC and CNF surfaces were determined by conductometric titration assays adapted from

published methods.<sup>39–41</sup> Zeta potentials were measured in a broad range of pH values (1–13). Dispersion flow curves (shear viscosity) and dynamic shear properties (storage modulus  $G'$  and loss modulus  $G''$ ) were measured by using a modular advanced rheometer system. The detailed procedures are presented in [Supporting Information](#).

**Tensile Properties of Self-Standing TO-CNF Films.** Films containing TO-CNFs from leaves (L), stems (S), or combinations of both (LS) were prepared via solvent casting according to the formulations listed in [Table 1](#).

**Table 1. TO-CNF Film Composition on a Dry Basis**

film	TO-CNFs from leaves/wt %	TO-CNFs from stems/wt %
L-TO-CNF	100	0
S-TO-CNF	0	100
LS-TO-CNF 1:1	50	50
LS-TO-CNF 2:1	67	33
LS-TO-CNF 3:1	75	25

The tensile properties of self-standing films were tested as described in [Supporting Information](#).

## RESULTS AND DISCUSSION

**Influence of Cellulose Anatomical Origin and Production Methods on the Lignin Content, Crystallinity, and Conversion Yields of Nanocelluloses.** The main treatments performed in this study are schematically summarized and shown in [Figure 1](#). The leaves and stems of elephant grass were equally pretreated via a sequential acid–alkaline process ([Figure 1B](#)). This procedure increased the cellulose content in the substrates from 32 and 36% to up to 80 wt % ([Table S1](#)). The chemical composition of the pretreated leaves and stems was, respectively, cellulose ( $81 \pm 2$  and  $76.6 \pm 0.2$  wt %), hemicellulose ( $4.0 \pm 0.3$  and  $3.1 \pm 0.1$  wt %), lignin ( $7.7 \pm 0.4$  and  $12 \pm 1$  wt %), ash ( $0.8 \pm 0.3$  and  $0.5 \pm 0.1$  wt %), and extractives ( $8.2 \pm 0.1$  and  $6.3 \pm 0.3$  wt %). Hemicellulose and lignin removal imparted a lighter color to the lignocellulosic biomass and a morphology formed by

thinner particles ([Figures 1](#) and [S1](#)). The extraction of these components contributes to overcome biomass recalcitrance, favoring the deconstruction and defibrillation of the plant cell wall.<sup>32,42</sup> As shown in [Figure S2](#), the pretreatments enhanced the fiber fragmentation and surface micrometric texture, which can promote the accessibility toward cellulose microfibrils and likely improve nanocellulose production from cellulose-enriched substrates.<sup>43,44</sup>

The cellulose-enriched substrates were converted into nanocelluloses through two different routes: (1) acid hydrolysis and (2) TEMPO-oxidation, followed by sonication. In addition to AH-CNCs, AH-CNFs were recovered as precipitated, partially hydrolyzed coproducts of the sulfuric acid hydrolysis ([Figure 1C](#)) with yields up to 37% ([Table 2](#)). Because this method is the most conventional and scalable approach to obtain CNCs,<sup>45</sup> valorizing process residues such as precipitated nanofibrils would be strongly beneficial to promote the integral use of lignocellulosic resources.<sup>32</sup> On the other hand, TEMPO-oxidation/sonication ([Figure 1D](#)) yielded both TO-CNFs and TO-CNCs by simply changing the sonication time. This method has been explored as an acid-free alternative to produce both nanofibrils and nanocrystals by varying oxidation severity<sup>12</sup> and/or sonication times.<sup>13</sup> Zhou et al.<sup>13</sup> showed that cavitation for 30 min resulted in long nanoelements with or without kinks, while 60 and 120 min sonication yielded needle-like nanocrystals with equally high carboxylate contents. Therefore, while fibrillating microfibril bundles, this time-dependent procedure probably promotes the perpendicular cleavage of individualized oxidized microfibrils first into flexible nanofibrils and then into rigid rodlike nanocrystals.<sup>12</sup> One of its main advantages is the absence of energy-consuming mechanical steps after oxidation (e.g., microfluidic homogenization, grinding, or refining) once fibrillation is achieved by simple and cost-effective probe-sonication. Both acid hydrolysis and TEMPO-oxidation are particularly suitable for the conversion of grass biomasses, such as elephant grass<sup>32</sup> or sugarcane bagasse,<sup>12</sup> into nanostructures.

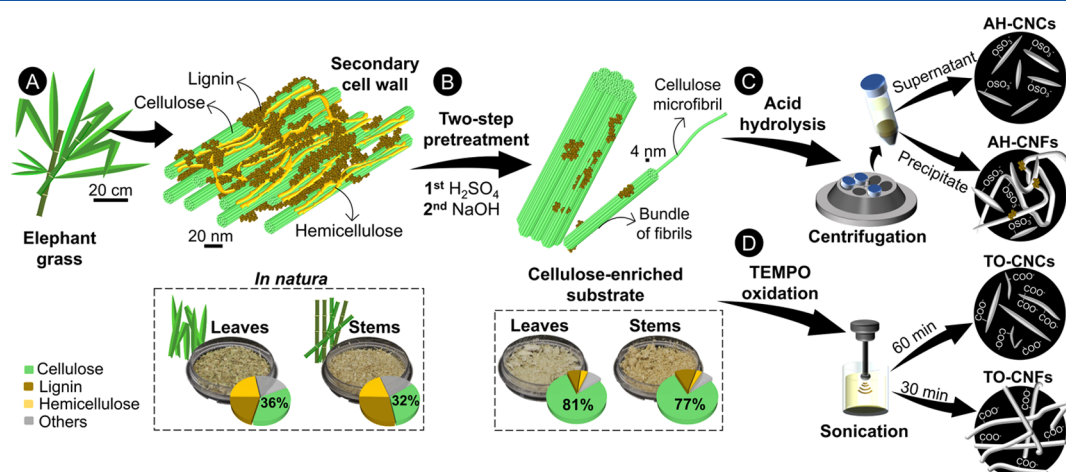


**Figure 1.** Depiction of the processing methods used to obtain CNCs and CNFs. (A) Elephant grass leaves and stems are composed mainly of cellulose, hemicellulose, and lignin. (B) After an acid pretreatment with diluted H<sub>2</sub>SO<sub>4</sub>, followed by an alkaline step with diluted NaOH, most of hemicellulose and lignin were removed, resulting in cellulose-enriched substrates. (C) Pretreated substrates from leaves or stems underwent hydrolysis with concentrated H<sub>2</sub>SO<sub>4</sub> so that AH-CNCs could be obtained as a turbid supernatant after centrifugation/rinsing cycles with water, and AH-CNFs were recovered as the precipitate remaining after centrifugation. (D) Alternatively, cellulose-enriched substrates underwent TEMPO-mediated oxidation, followed by centrifugation/rinsing steps (omitted) and sonication for 30 min, yielding TO-CNFs, or 60 min, yielding TO-CNCs dispersed in water.

Table 2. Conversion Yields of CNCs and CNFs Produced Using Different Methods and Plant Anatomical Parts<sup>a</sup>

nanocellulose	method	source	plant part	yield/%	refs
CNCs	acid hydrolysis	elephant grass	leaves	70 ± 2	<sup>b</sup>
	TEMPO/sonication	elephant grass	leaves	65 ± 2	<sup>b</sup>
	acid hydrolysis	elephant grass	stems	28 ± 2	<sup>b</sup>
	TEMPO/sonication	elephant grass	stems	72 ± 3	<sup>b</sup>
	acid hydrolysis	elephant grass	leaves	53 ± 2	32
	acid hydrolysis	eucalyptus pulp	trunks (stems)	75.6	56
	TEMPO/sonication	microcrystalline cellulose	-	70.0	13
	acid hydrolysis	African grass (Diss)	stems	8–9	54
	TEMPO/sonication	softwood kraft pulp	trunks (stems)	94	13
	acid hydrolysis	cotton pulp	flower	64 ± 1	53
	TEMPO/sonication	sugarcane	bagasse	59	12
	TEMPO/sonication	oil palm biomass	fruit bunch	93.0	57
	CNFs	acid hydrolysis	elephant grass	leaves	22 ± 4
TEMPO/sonication		elephant grass	leaves	65 ± 2	<sup>b</sup>
acid hydrolysis		elephant grass	stems	37 ± 2	<sup>b</sup>
TEMPO/sonication		elephant grass	stems	72 ± 3	<sup>b</sup>
acid hydrolysis		elephant grass	leaves	26 ± 9	32
TEMPO/sonication		sugarcane	bagasse	94	12
TEMPO/sonication		sugarcane	bagasse	57	12
TEMPO/sonication		oil palm biomass	fruit bunch	99	57

<sup>a</sup>Yields are relative to pre-hydrolysis or pre-oxidation substrate weight. <sup>b</sup>Yields obtained in the present work.

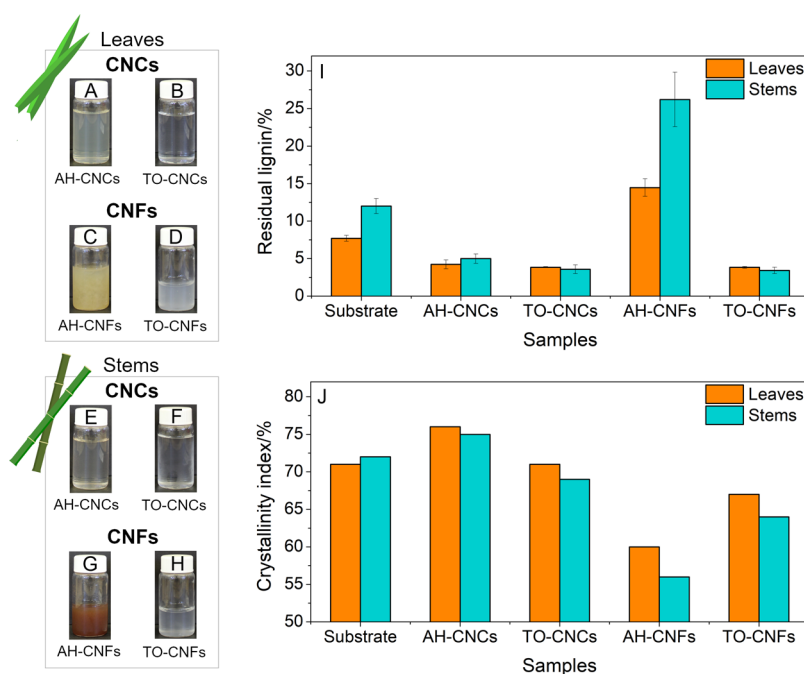


**Figure 2.** Photographs under visible light of aqueous dispersions of nanocelluloses obtained from (A–D) leaves and (E–H) stems of elephant grass. (I) Residual lignin content and (J) crystallinity index of cellulose-enriched substrates, CNCs, and CNFs.

As shown in Figure 2A–H, aqueous dispersions of AH-CNCs, as well as TO-CNCs and TO-CNFs, presented similar transparency/translucency and light coloration. Light transmittance in the visible range (at 600 nm) varied from *ca.* 90% in TO-CNCs to 69–76% in AH-CNCs and 65–68% in TO-CNFs (Figure S3 and Table S2). Fukuzumi et al.<sup>20</sup> reported light transmittances >80% at 600 nm for more diluted TO-CNF/water dispersions [0.15% (w/v) there vs 0.5% (w/v) here]. The decreased transmittance of AH-CNCs can be attributed to the presence of large aggregates, including entangled cellulosic structures and perhaps precipitated fragments of lignin. Likewise, the semitransparent aspect of

the TO-CNF dispersion can be associated with the presence of long fibrils and entangled networks larger than 400 nm. In contrast, systems containing leaf and stem AH-CNFs were opaque with low-light transmittance (<10%) and had a light brown and dark brown color, respectively. The difference in the visual aspects could be associated with the presence of different contents of residual lignin and should be considered in the final applications of these nanostructures, for example, in nanocomposite coatings or electronic devices, when color and transparency matter.

AH-CNFs were purified only to eliminate excess acid species, oligomers, glucose, and soluble degradation products.

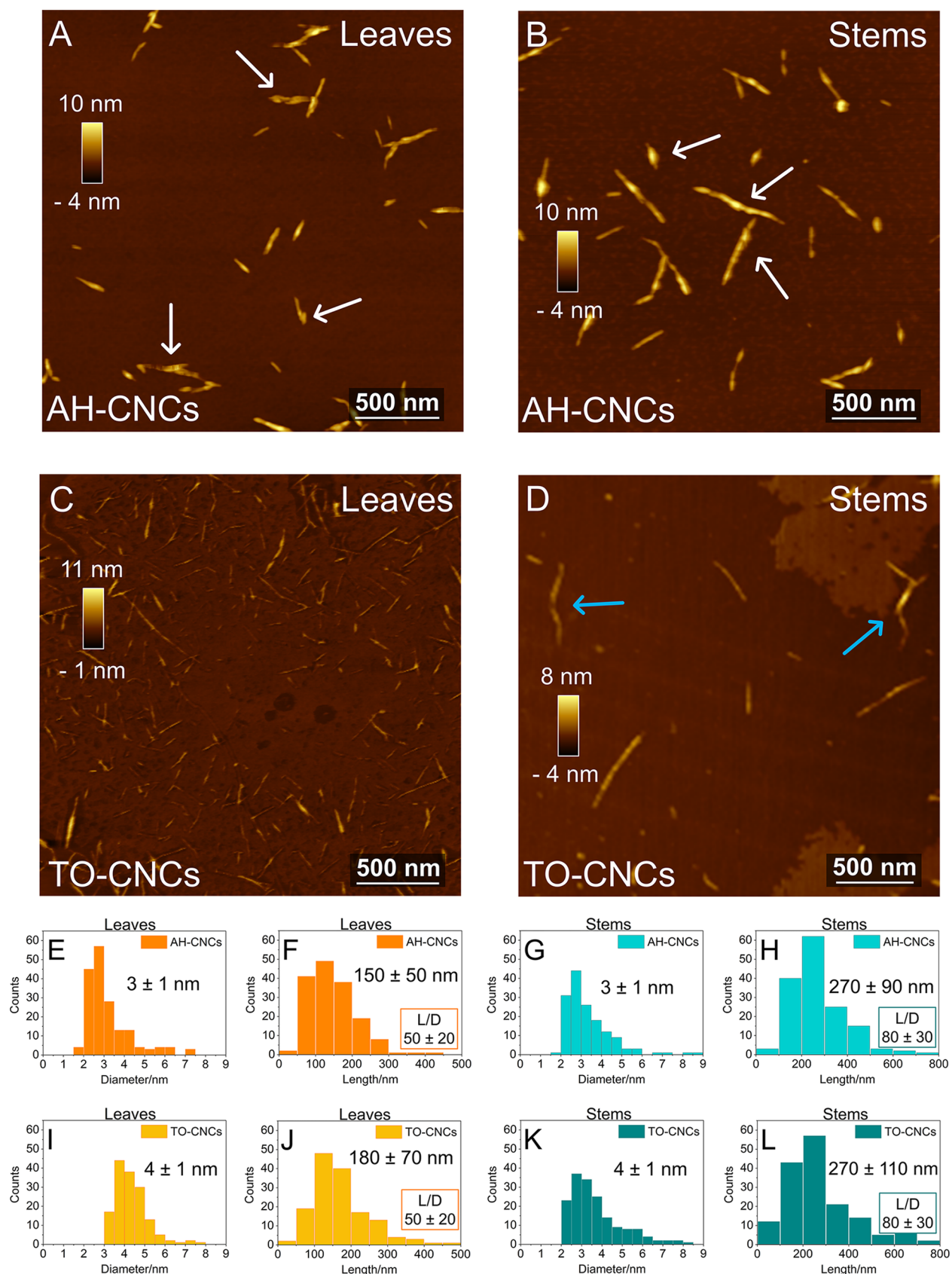


**Figure 3.** AFM topography micrographs of (A,B) AH-CNCs and (C,D) TO-CNCs produced from elephant grass leaves and stems. The white arrows in (A,B) indicate defects in AH-CNCs. The blue arrows in (D) indicate kinks in TO-CNCs. Size distribution histograms of the diameter and length calculated from AFM height images of (E–H) AH-CNCs and (I–L) TO-CNCs. At least 150 nanoparticles were measured in 4 different images per sample.

Therefore, they contained  $14 \pm 1$  and  $26 \pm 4$  wt % of residual lignin, respectively, in leaf and stem AH-CNFs (Figure 2I). Lignin percentages increased in these samples compared to their precursor substrates, though the absolute content of lignin decreased. Considering the nanocellulose production yields reported in Table 2, the lignin content decreased from 8 to 12 g in 100 g of starting cellulose-enriched substrates to 3–10 g in the prepared AH-CNFs. Such remaining aromatic macromolecules are likely condensed structures with high molecular weight, thus constituting recalcitrant lignin–carbohydrate complexes.<sup>46</sup> Negligible residual lignin contents could be achieved by performing more severe purification procedures prior to nanocellulose production, including harsh delignification (higher concentration, temperature, and time)<sup>47</sup> and/or multiple bleaching steps.<sup>12</sup> However, the preparation of lignin-containing CNFs is an advantageous rising trend because the presence of residual lignin can enhance CNF thermal and interfacial behavior,<sup>22</sup> also providing additional properties, such as UV-absorption,<sup>23</sup> antioxidant, and antimicrobial abilities<sup>46</sup> to nanocomposites and other advanced materials.

The amorphous nature of lignin likely contributed to the lower CrI of lignin-containing AH-CNFs when compared to the substrates and other nanocellulose samples (Figure 2J). While the sequential acid–alkaline pretreatment increased the crystallinity of leaves and stems from 53 and 63 to 71 and 72%, respectively (Figure S4), AH-CNFs presented a CrI as small as 56%. In turn, AH-CNCs presented the highest crystallinity of up to 76% and less than 5% of residual lignin. An equivalent CrI (76%) was previously reported for AH-CNCs extracted from the same biomass.<sup>32</sup> This result is also in accordance with the acid hydrolysis process used to prepare these samples, which separated the most crystalline fractions (AH-CNCs) from the less crystalline fractions (AH-CNFs). Furthermore, regardless of the production method or the plant anatomical origin, CNCs showed greater crystallinity than CNFs.

TO-CNFs presented a CrI of 64–67%, which was also lower than the crystallinity of the original cellulose-enriched substrates. Daicho et al.<sup>48</sup> reported a reduction in the CrI of TEMPO-oxidized softwood dissolving pulp from 48 to 22% after wet disintegration into TO-CNFs. This phenomenon was attributed to the increase in the specific surface area and the conformational changes of partly crystalline surfaces to noncrystalline surfaces when fibrils are cleaved longitudinally, detached, and then dispersed as TO-CNFs.<sup>49</sup> Differently, for TO-CNCs, the CrI increased to ca. 70%, as previously observed for wheat straw cellulose, whose crystallinity increased from 66 to 79% with sonication.<sup>50</sup> In this case, further cavitation, with increasing local system temperature and pressure, probably promoted the preferential cleavage and degradation of amorphous cellulose regions while causing only little damage to the crystalline regions.<sup>51</sup> Therefore, the contribution of lignin to the decrease in crystallinity was negligible for these samples.

TO-CNFs and TO-CNCs presented ca. 3.5% of residual lignin on a dry weight basis, while TEMPO-oxidized wood pulps usually contain very low amounts of residual lignin (less than 1%).<sup>52</sup> The relatively high lignin concentration in the nanocelluloses produced from elephant grass can be attributed to the effects of the mild pretreatments performed, as well as to the types and contents of lignin that remained in the cellulose-enriched substrates after such pretreatments.

Table 2 shows the conversion yields on a dry weight basis for all the samples studied here and the comparison of these yields with those of different studies in which cellulose-enriched substrates were converted into cellulose nanostructures. The hydrolysis of pretreated leaves yielded  $70 \pm 2\%$  of AH-CNCs and  $22 \pm 4\%$  of coproduced AH-CNFs. These yields were comparable to values reported for the same biomass under similar pretreatment and hydrolysis conditions<sup>32</sup> as well as for processed pulps under optimized conditions of concentration and reaction time during sulfuric acid hydrolysis.<sup>53</sup> For stems, the hydrolysis efficiency of the conversion into AH-CNCs and AH-CNFs was lower ( $28 \pm 2$  and  $37 \pm 2\%$ , respectively), indicating the occurrence of incomplete hydrolysis. Luzi et al.<sup>54</sup> also reported low reaction efficiency (8.7%) for the sulfuric acid hydrolysis of *Diss* (*Amplodesmos mauritanicus*) stems into CNCs. These results suggest that stems are more recalcitrant than leaves and indicate that increasing the severity of stem hydrolysis conditions (temperature, time, or acid concentration) could improve the yields.

Additionally,  $65 \pm 2\%$  of the cellulose-enriched substrate from leaves and  $72 \pm 3\%$  from stems were recovered as TO-CNFs after 30 min of sonication and then as TO-CNCs after 60 min of sonication. These weight recovery ratios were comparable to values reported for nanocelluloses produced from microcrystalline cellulose<sup>13</sup> and sugarcane bagasse oxidized with high concentrations of the oxidizing agent.<sup>12</sup> Nevertheless, the results obtained here were lower than values reported for various biomasses under milder oxidation,<sup>12,13</sup> whose recovery yields exceeded 90%.

Weight losses during TO-CNC and TO-CNF production can be attributed to the removal of lignin, hemicellulose, and amorphous cellulose as water-soluble fractions.<sup>52,55</sup> In fact, Pinto et al.<sup>12</sup> and Okita et al.<sup>52</sup> showed that increasing the severity of TEMPO-mediated oxidation reduced the recovery ratios. Herein, the concentration of the oxidizing agent,  $60 \text{ mmol g}^{-1}$ , was higher than the condition usually reported in the literature,  $5 \text{ mmol g}^{-1}$ .<sup>4</sup> The experimental trials indicated that low NaClO concentration was not sufficient to promote efficient fibrillation of elephant grass by sonication after just a mild dilute acid–alkaline pretreatment. Relatively high residual lignin content prompted the demand for a harsh oxidation procedure. This grass is not particularly recalcitrant compared to wood biomasses but has greater recalcitrance than processed biomasses such as sugarcane bagasse, which could be effectively fibrillated by sonication after oxidation with  $50 \text{ mmol g}^{-1}$  sodium hypochlorite.<sup>12</sup>

### Influence of the Cellulose Anatomical Origin and Production Methods on Nanocellulose Morphology.

AH-CNCs and TO-CNCs presented typical nanocrystal morphology, with a rodlike shape, as shown by AFM and TEM micrographs (Figures 3A–D and S5). In needle-shaped AH-CNCs, there were sharp, narrower extremities, as well as apparent defects along the longitudinal direction. These irregularities could be attributed to the former amorphous zones transversely degraded and cleaved during acid hydrolysis.<sup>5</sup> TO-CNCs, on the other hand, presented smoother laterals, despite the presence of some defects and small kinks. These twists and kinks were remaining amorphous zones,<sup>43</sup> whose presence likely contributed to the lower CrI of TO-CNCs (69–71%) when compared to AH-CNCs (75–76%, Figure 2J).

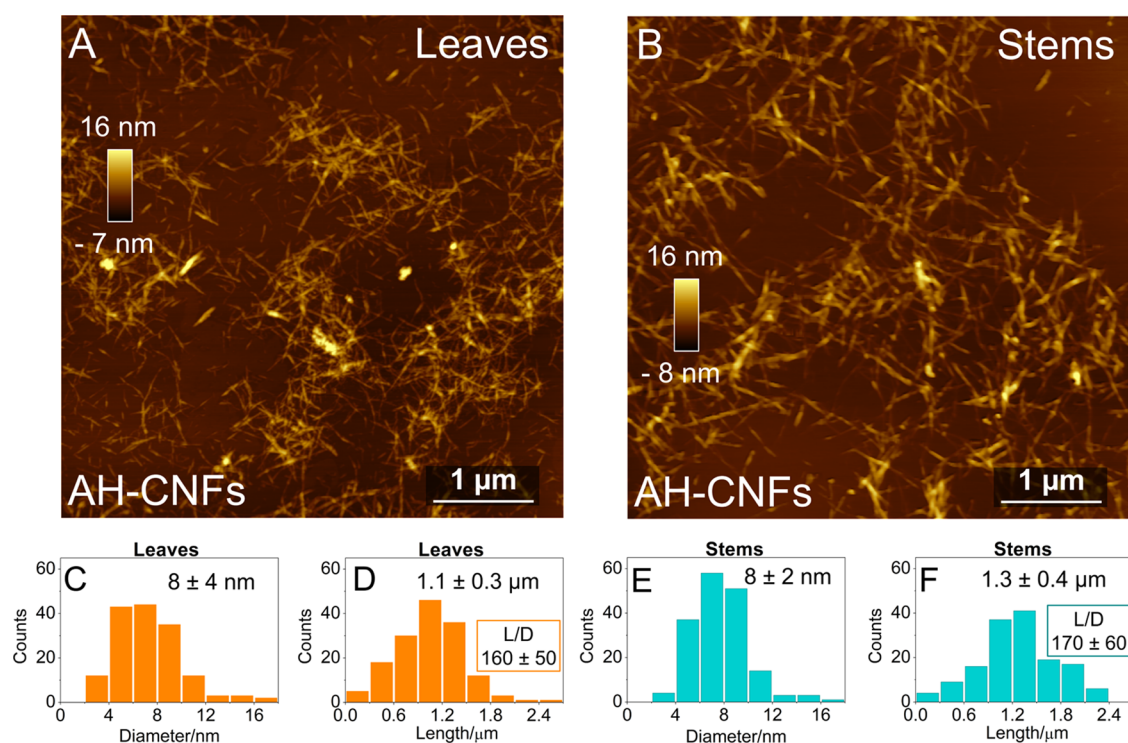


**Figure 4.** AFM topography micrographs of AH-CNFs from (A) leaves and (B) stems. Size distribution histograms of the diameter and length calculated from AFM height images of AH-CNFs from (C,D) leaves and (E,F) stems. At least 150 nanoparticles were measured in 4 different images per sample.

All CNCs presented skewed size distributions in the nanoscale (Figure 3E–L). The average diameters of AH-CNCs,  $3 \pm 1$  nm, and TO-CNCs,  $4 \pm 1$  nm, were virtually equivalent and correspond to the crystallite diameter of the cellulose elementary fibril in vascular plants, such as grasses. The cross-sectional width of the fibril is estimated as 2–3 nm or less than 36 cellulose chains.<sup>58</sup>

Average lengths, contrariwise, depended on the plant anatomical part from which cellulose was extracted. Independent of the production method, CNCs from stems were significantly longer than CNCs from leaves. The size distribution of the latter was skewed for lengths shorter than 200 nm (Figures 3F,J and S5), while the opposite was verified for CNCs from stems (Figure 3H,L). The dimensions of leaf CNCs were comparable to the lengths of AH-CNCs extracted from elephant grass leaves,  $167 \pm 45$  nm,<sup>32</sup> and TO-CNCs produced from sugarcane bagasse,  $159 \pm 71$  nm.<sup>12</sup> Sulfated and carboxylated CNCs extracted from *Juncus* plant stems also presented large average lengths of  $431 \pm 94$  and  $352 \pm 79$  nm, respectively.<sup>11</sup>

Accordingly, the aspect ratio ( $L/D$ , length-to-diameter ratio) of stem CNCs was significantly greater than that of leaf CNCs. For AH-CNCs, the aspect ratio depends on the cellulose source and, mainly, on the conditions and severity of the hydrolysis performed.<sup>6</sup> Considering the single hydrolysis condition used here, the results presented so far evidenced that the cellulose anatomical origin played an important role in determining the morphological features of both AH-CNCs and TO-CNCs.

Concerning the production of nanofibrils, the anatomical origin of cellulose proved to be more important when TEMPO-mediated oxidation/sonication was used than when CNFs were obtained by acid hydrolysis. AH-CNFs obtained

from leaves or stems showed elongated morphology, forming nanofibrillated networks, as shown in Figure 4A,B. Their average diameter was estimated as *ca.* 8 nm, with a diffuse skewed distribution (Figure 4C,E). There was a tendency of predominant lengths greater than 1.2  $\mu\text{m}$  for stem AH-CNFs and the opposite for leaf AH-CNFs (Figure 4D,F), but the averages were virtually equivalent. In addition, the difference in the aspect ratio of these two samples was not statistically significant.

Differently, the average length of stem TO-CNFs (Figure 5H) was significantly larger than that of leaf TO-CNFs (Figure 5F). Cellulose biosynthesis in leaves, which are largely occupied by mesophyll cells, that is, thin-walled parenchymatic tissues,<sup>59</sup> contributed to the production of shorter, straighter, and randomly entangled TO-CNFs (Figure 5A,C). Stems, on the other hand, grow from the elongation of individual cells,<sup>60</sup> generating more elongated and curled morphology in TO-CNFs (Figure 5B,D), with common lengths greater than 1  $\mu\text{m}$  (Figures 5H and S6). The hierarchical biosynthetic pathway during elongation does not influence the fibril diameter, which remains constant, ranging from 2 to 20 nm depending on the cellulose source.<sup>3,60</sup> Accordingly, the diameters of TO-CNFs from leaves and stems were virtually equivalent (Figure 5E,G), and the aspect ratios of TO-CNFs from stems were greater than those from leaves, as previously observed for CNCs.

**Influence of the Anatomical Origin and Production Methods on Chemical Properties, Colloidal Stability, and Rheology of Nanocelluloses.** The anatomical origin also had a remarkable effect on the degree of polymerization of the produced nanocelluloses. The initial  $\text{DP}_v$  values of cellulose-enriched substrates from leaves and stems were  $920 \pm 10$  and  $1020 \pm 6$ , respectively. As shown in Figure 6A, leaf

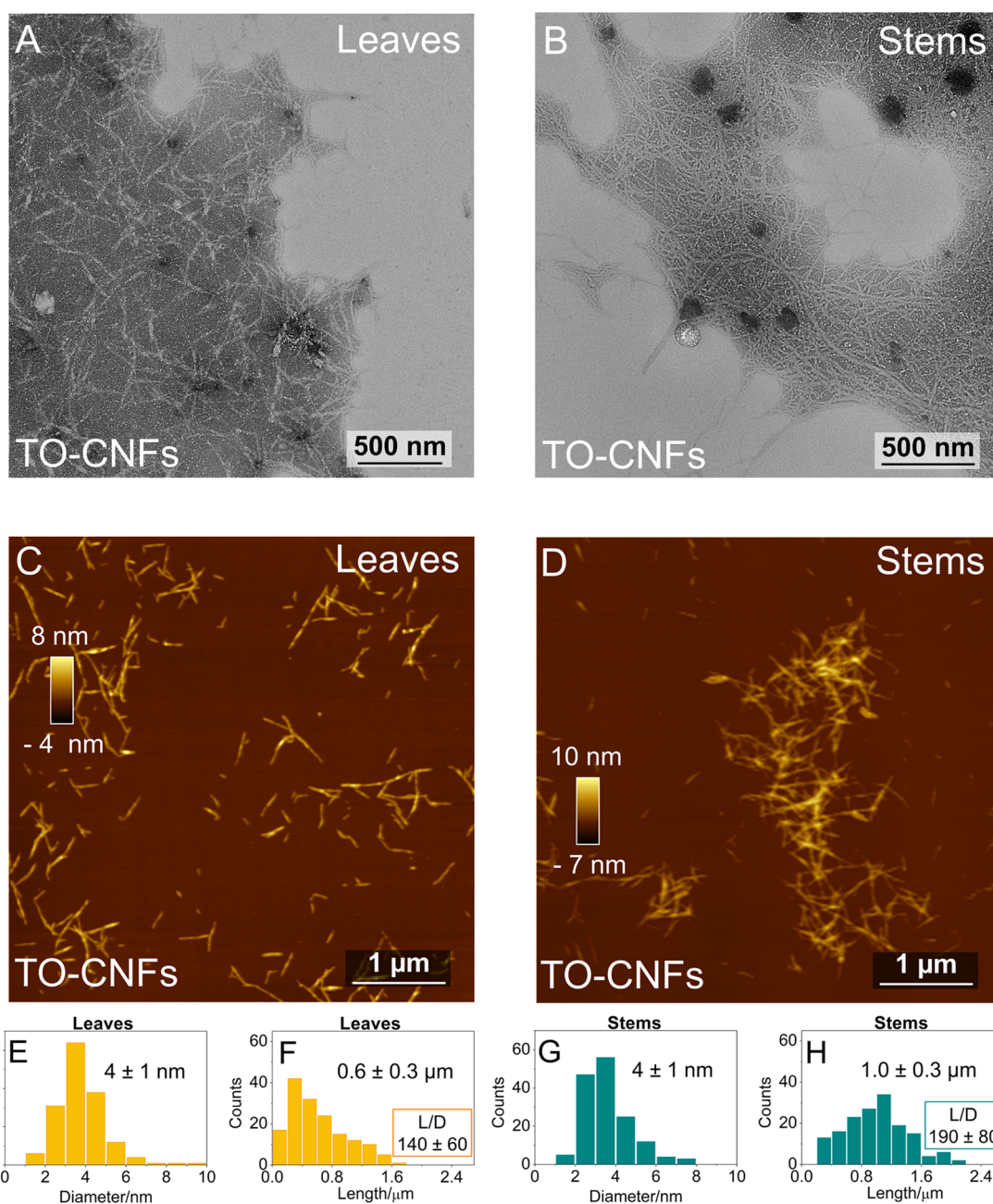


**Figure 5.** (A,B) TEM and (C,D) AFM micrographs of TO-CNFs from leaves and stems. Size distribution histograms of the diameter and length calculated from AFM height images of TO-CNFs from (E,F) leaves and (G,H) stems. At least 150 nanoparticles were measured in 4 different images per sample.

CNCs presented a  $DP_v$  of about 100, and stem CNCs showed a  $DP_v$  of up to 200, independent of the preparation method.

In general, cleavages induced by acid hydrolysis cause a rapid reduction of cellulose  $DP_v$  to its levelling-off degree of polymerization (LODP).<sup>3</sup> The LODP is usually correlated to the longitudinal dimension of native cellulose crystals and depends on the plant source. For example, Battista et al.<sup>61</sup> reported LODP values of 200–250 for cotton fibers and 80–280 for treated wood pulps. Hence, the  $DP_v$  measured here for CNCs from leaves and stems is likely the LODP of cellulose in these two parts of the grass.

Also,  $DP_v$  of CNFs was higher than that of CNCs (Figure 6A), especially in samples prepared via acid hydrolysis. Shinoda and co-workers<sup>37</sup> reported a linear relationship

between  $DP_v$  and the length-weighted average length of TO-CNFs. Accordingly, CNFs from stems were longer and presented significantly greater  $DP_v$  than CNFs produced from leaves. The influence of the production method was noticeable in  $DP_v$  of CNFs mainly. Leaf and stem AH-CNFs, which were slightly longer and thicker than the corresponding TO-CNFs, had higher  $DP_v$  values. The lower  $DP_v$  values measured for TEMPO-oxidized nanocelluloses can also be influenced by the depolymerization of cellulose during dissolution in CED at high pH ( $\sim 14$ ) due to the presence of unconverted C6-aldehyde intermediates.<sup>37</sup> Nevertheless, Fukuzumi et al.<sup>20</sup> reported comparable  $DP_v$  values of 350 and 400 for TO-CNFs with length-weighted average lengths of 680 and 1100 nm, respectively.

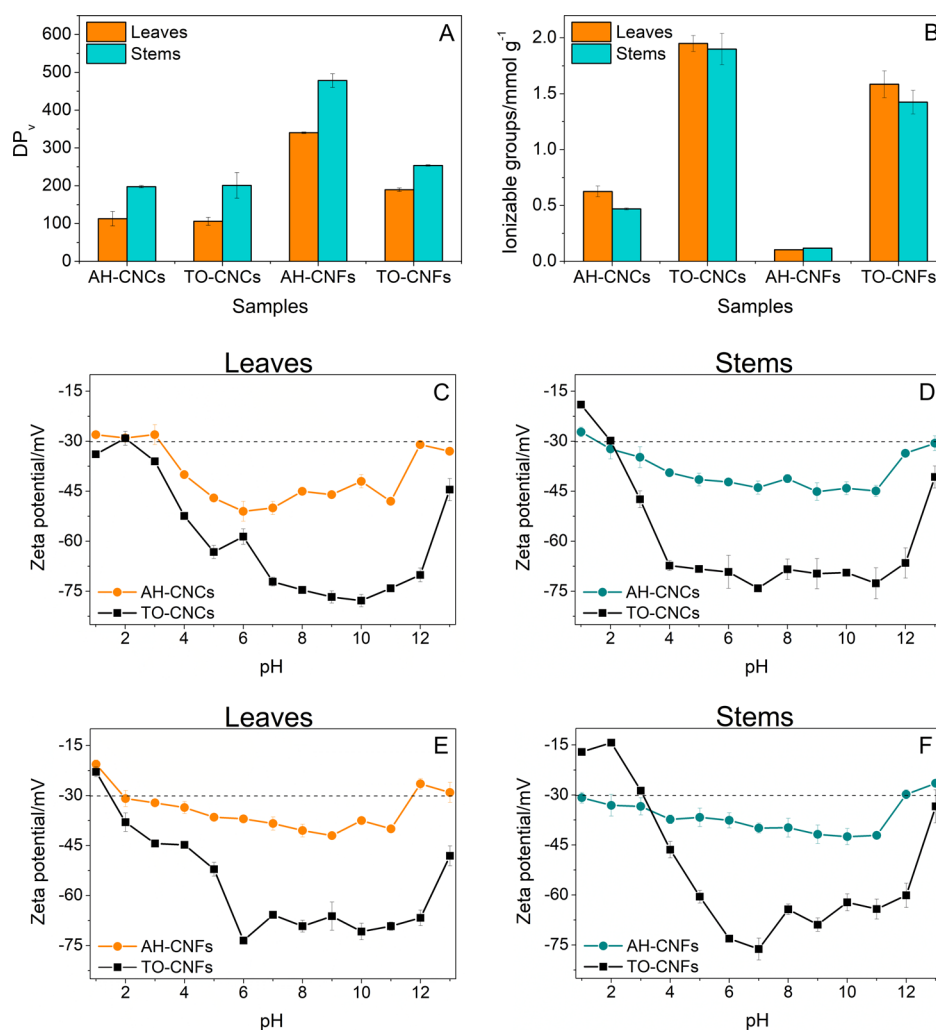


**Figure 6.** (A)  $DP_v$  measured for CNCs and CNFs from leaves and stems. (B) Content of ionizable groups estimated by conductometric titration of CNC and CNF dispersions. Zeta potential as a function of pH (1–13) for (C,E) leaf and (D,F) stem CNC and CNF dispersions. The dotted lines delimitate the value of  $-30$  mV in the y-axis.

The preparation approach was also of paramount relevance for the surface chemistry of CNCs and CNFs. In fact, sulfuric acid hydrolysis and TEMPO-mediated oxidation imparted different amounts of ionizable groups and surface charge densities to the nanocelluloses. As shown in Figure 6B, the conductometric titration of weak acids indicated the presence of high concentrations of carboxylic acid/carboxylate groups in TEMPO-oxidized nanocelluloses (up to  $1.9 \text{ mmol g}^{-1}$  of TO-CNCs and  $1.6 \text{ mmol g}^{-1}$  of TO-CNFs). The conductometric titration of strong acids, in turn, indicated the presence of sulfate half-ester groups on the surface of AH-CNCs in concentrations of up to  $0.6 \text{ mmol g}^{-1}$ . In AH-CNFs, the content was about  $0.1 \text{ mmol g}^{-1}$ . The common ranges of surface charge densities are  $0.08\text{--}0.35 \text{ mmol g}^{-1}$  of AH-CNCs,  $0.1\text{--}3.5 \text{ mmol g}^{-1}$  of TO-CNCs, and  $0.2\text{--}1.8 \text{ mmol g}^{-1}$  of TO-CNFs.<sup>62</sup>

All aqueous dispersions were stabilized by electrostatic repulsion between nanoparticles over wide pH ranges, as indicated by zeta potential measurements (Figure 6C–F). Because TEMPO-mediated oxidation imparted higher amounts of anionic groups onto the surface, TO-CNCs and TO-CNFs presented greater surface charge densities and zeta potentials well below  $-30$  mV, from pH 2–3 to 13. Even AH-CNFs, with the lowest content of ionizable groups among the

samples, presented negative zeta potentials, albeit close to  $-30$  mV, ranging from pH 2 to 11. This feature is highly important in determining the shelf life and pH-controlling stability parameters of water-based formulations containing nanocelluloses.

The  $pK_a$  values of C6 carboxyl and sulfate groups are, respectively, *ca.* 3.6 and 1.9.<sup>63,64</sup> Therefore, the magnitude of zeta potentials decreased at very acidic pH values, as protonation occurs due to the addition of excess  $H^+$ . The surface charge becomes insufficient to ensure the colloidal stability, that is, the electrostatic repulsion can no longer overcome attractive forces between nanoparticles, such as hydrogen bonding and van der Waals interactions. On the other hand, at pH 12–13, nanoparticles also lacked colloidal stability due to the screening or electrostatic shielding effect of the added counterions.<sup>65</sup>

As shown by the flow curves (shear viscosity as a function of the shear rate) in Figure 7A,B, all CNC and CNF dispersions at a concentration of 2% (w/v) (equivalent to 1.3% v/v) exhibited typical non-Newtonian shear-thinning behavior.<sup>66</sup> Rodlike particles or fibrils in aqueous dispersions tend to be aligned and partly disentangled by the flow, becoming less viscous as the shear rate increases.<sup>19</sup> The percolation threshold of the nanoparticles in deionized water was determined

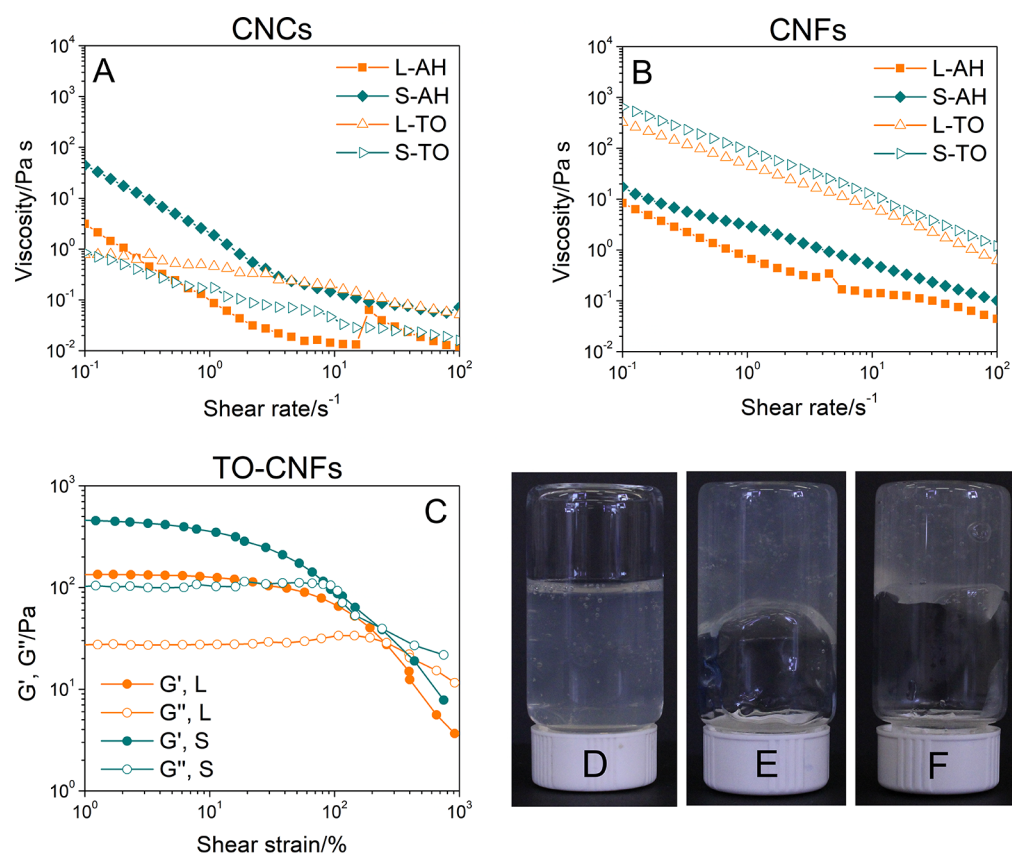


**Figure 7.** Representative curves of steady shear viscosity as a function of the shear rate for (A) CNCs and (B) CNFs in aqueous dispersions (2% w/v). L refers to nanostructures extracted from leaves and S refers to nanostructures extracted from stems. (C)  $G'$  and  $G''$  as a function of the shear strain amplitude for L- and S-TO-CNFs. Photographs under visible light of dispersions of (D) L-TO-CNCs, (E) L-TO-CNFs, and (F) S-TO-CNFs, showing that (E) and (F) form invertible gels at a concentration of 2% (w/v).

considering their aspect ratio and varied from 1.4% (v/v) in CNCs from leaves to less than 0.8% (v/v) in all the other samples (Table S3). Therefore, except for leaf AH-CNCs and TO-CNCs, the nanocelluloses likely formed percolated networks in dispersions.

At low shear rates, TO-CNCs presented the smallest viscosities ( $10^{-1}$ – $10^0$  Pa s), while TO-CNFs presented the highest viscosities ( $10^2$ – $10^3$  Pa s). The measured viscosities were comparable to the values reported by Liao et al.<sup>67</sup> for dialyzed CNCs (ca.  $10^{-1}$  Pa s) and TO-CNFs ( $10^1$ – $10^2$  Pa s) at equivalent concentrations. Analogously, the particle length/aspect ratio also played an important role in determining the viscosity of the dispersions,<sup>19</sup> as a clear tendency of increased shear viscosity for nanostructures extracted from stems was observed for AH-CNCs, AH-CNFs, and TO-CNFs. For TO-CNCs (Figure 7D), this tendency was not verified, probably due to the concurrent effect of the very high surface charge. For comparison, while both AH-CNCs and TO-CNCs showed similar steady viscosity behavior, with a shear-thinning region, then plateaus followed by another shear-thinning region,<sup>67</sup> the slope of the shear-thinning region of TO-CNCs was much smaller.

However, for the acid hydrolyzed nanocelluloses, the presence of a significant amount of residual lignin also may be considered. Though they were longer, stem AH-CNFs presented slightly lower viscosity than stem AH-CNCs. Studies by Yuan et al.<sup>25</sup> showed that at the same concentration level and shear rate, CNFs containing a lower amount of residual lignin (ca. 6%) presented the highest viscosity, while CNFs

containing a higher amount of residual lignin (ca. 24%) presented the lowest viscosity. These contents of residual lignin and viscous behavior agree with the characteristics presented by stem AH-CNCs (270 nm, ca. 5% residual lignin, and high viscosity) and stem AH-CNFs (1300 nm, ca. 26% residual lignin, and almost equivalent viscosity). At intermediate lignin contents (10%), on the other hand, Iglesias et al.<sup>26</sup> reported similar flow curves to that presented by leaf AH-CNFs (14% residual lignin), with a transitional behavior near  $10$  s<sup>-1</sup> in which a remarkable change in viscosity was observed. For these samples, the fibril length and adequate lignin content acted concurrently in improving the dispersion viscosity in comparison to leaf AH-CNCs.

Conversely, TO-CNF dispersions formed invertible gels at 2% concentration (Figure 7E,F). When the dispersions underwent oscillatory shear strain (Figure 7C),  $G'$  and  $G''$  values taken from the amplitude strain sweep confirmed that, as verified in the flow curves, stem TO-CNFs, which presented higher shear viscosity, also showed higher storage and loss moduli. While both leaf and stem nanoparticles have the same surface functionalities and content of ionizable groups, the differences observed are likely due to the distinct specific surface area and degree of entanglement,<sup>66</sup> revealing the relevance of the particle length and aspect ratio to the rheological properties of CNF dispersions. Therefore, considering cellulose biosynthesis could be useful while tailoring the viscoelastic behavior of CNFs in coating formulations or biomedical hydrogels, for instance. As previously reported for TEMPO-oxidized CNFs in comparison to long CNCs,<sup>19</sup> in the

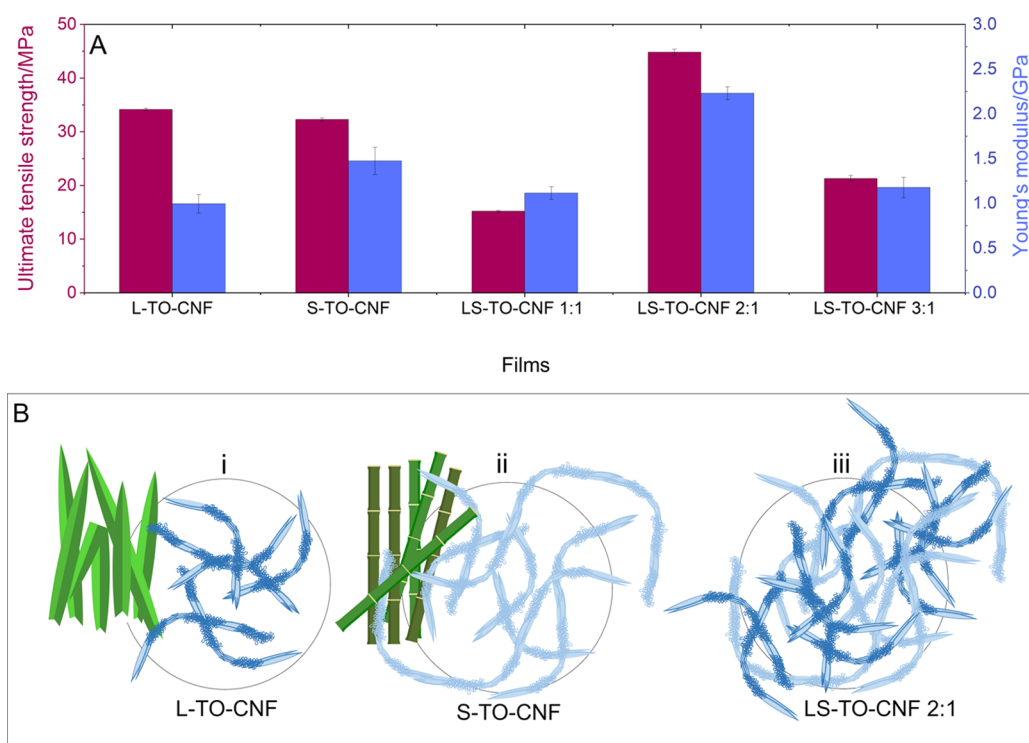


**Figure 8.** (A) Ultimate tensile strength (left axis) and Young's modulus (right axis) for films of TO-CNFs from leaves, stems, and 1:1, 2:1, and 3:1 blends. (B) Schematic diagram of the morphological arrangement of (i) L-TO-CNF, (ii) S-TO-CNF, and (iii) LS-TO-CNF 2:1.

linear viscoelastic region, that is, the region in which the moduli are independent of the applied shear strain,  $G'$  is greater than  $G''$ , indicating a gel-like behavior. At strain amplitudes higher than 100%, a critical state was reached, and both the moduli started to decrease nonlinearly until the magnitude of both was inverted ( $G'' > G'$ ), phenomenological evidence of the breakdown or disruption of the elastic network formed by TO-CNFs.<sup>19,66</sup>

Finally, Table S4 summarizes the key characteristics and physicochemical, morphological, and rheological differences between CNCs and CNFs from plant leaves or stems produced by acid hydrolysis or TEMPO-mediated oxidation, followed by sonication.

**Improved Tensile Mechanical Properties of Self-Standing Films Containing TO-CNFs from Leaves and Stems.** As previously discussed, the morphology and size of TO-CNFs from leaves and stems diverged greatly, also implying differences in the dynamic moduli of CNF aqueous dispersions. The effect of this difference on the tensile mechanical properties of self-standing TO-CNF thin films was evaluated. Leaf and stem TO-CNFs were tested separately or in combined systems, which were transparent and homogeneous (Figure S7) and presented an average thickness of  $27 \pm 5 \mu\text{m}$ . When combined in a 2:1 leaf-to-stem ratio, the films were visually regular and flat.

Furthermore, the brittle LS-TO-CNF 2:1 film showed significantly higher ultimate tensile strength (about 45 MPa) and stiffness (Young's modulus of more than 2.2 GPa) than the single L- or S-TO-CNF films, as well as LS-TO-CNF 1:1 or 3:1 films (Figure 8A). Films prepared with partially disintegrated TEMPO-oxidized wood presented a comparable tensile strength of 43 MPa and Young's modulus of 1.9 GPa.<sup>68</sup> The improved behavior of the combined system could be attributed to the favorable interpenetration and entanglement

as well as the existence of more contact points for the interaction between interconnected, shorter (600 nm) leaf TO-CNFs and neatly defined, longer (1000 nm) stem TO-CNFs (Figure 8B). Likewise, as shown in Table S5, although all the films presented similar water content (*ca.* 8–9%), the LS-TO-CNF 2:1 film exhibited slightly higher film density ( $1.06 \pm 0.01 \text{ g cm}^{-3}$ ) than the other self-standing films (*ca.* 0.91 to  $1.02 \text{ g cm}^{-3}$ ). The higher density likely contributed to the higher elastic modulus of this composite sample, as previously described.<sup>20</sup>

When comparing self-standing films based on TO-CNFs of different lengths but extracted from a single biosource (respectively, softwood and hardwood bleached kraft pulp), Fukuzumi et al.<sup>20</sup> and Saito et al.<sup>69</sup> concluded that longer CNF (1100–2000 nm) films presented higher densities ( $1.43$ – $1.47 \text{ g cm}^{-3}$ ), tensile strength (up to 266–312 MPa), and elastic modulus (up to 9.8–6.5 GPa) than shorter CNF (680–500 nm) films. Such films presented slightly lower densities ( $1.42$ – $1.45 \text{ g cm}^{-3}$ ), tensile strength (222–257 MPa), and Young's modulus (9.4–6.2 GPa). However, to the best of our knowledge, the promising combination of CNFs with different lengths in all-nanocellulose films, as introduced here, has not been reported before. This simple strategy, encompassing the use of a single production process on a single biomass resource (but different cellulose anatomical origins), potentially allows for tailoring the tensile mechanical properties of self-standing and nanocomposite TO-CNF films.

## CONCLUSIONS

The systematic study of various morphological, physicochemical, colloidal, and rheological properties of CNCs and CNFs allowed us to determine which of them were mostly influenced by the preparation method or by the anatomical origin of cellulose. The production method (sulfuric acid hydrolysis or

TEMPO-mediated oxidation, followed by sonication) affected all the properties to some extent, especially the crystallinity, zeta potential, and the content and type of ionizable groups onto the nanocellulose surface, implying an important contribution to the shelf life of water-based nanocellulose formulations. The crystallinity indices of acid-hydrolyzed CNCs (up to 76%) were higher than those of TEMPO-oxidized ones (up to 71%). In contrast, oxidized nanostructures from either leaves or stems showed higher content of ionizable groups (up to 1.95 mmol g<sup>-1</sup>) and colloidal stability (zeta potentials as negative as -76 mV).

Production yields, morphology, degree of polymerization, and rheological properties of nanocelluloses were influenced by both the production method and the anatomical origin. Due to cellulose biosynthesis, CNCs and CNFs from stems were longer and presented greater DP<sub>v</sub> than those from leaves. Additionally, the average length, diameter, and DP<sub>v</sub> of acid-hydrolyzed CNFs were greater than those of TEMPO-oxidized CNFs. The viscosity of these samples was highly influenced by both nanoparticle sizes and residual lignin content. Therefore, TEMPO-oxidized CNFs extracted from stems presented the highest steady shear viscosity and a pronounced gel-like behavior. Inherent differences between leaf and stem CNF morphology, length, and entanglement were explored by combining them in all-nanocellulose thin films, resulting in higher tensile strength and stiffness.

The structure–property relationships thoroughly discussed here can serve as a guideline during decision-making for both (1) the choice of methods and/or plant anatomical parts to produce nanocelluloses with tailored properties from several lignocellulosic biomasses and (2) the potential of combining different cellulose nanostructures to design advanced materials. Combinations of cellulose nanostructures obtained by different approaches or from different anatomical parts of a single biomass resource can potentially allow for the modulation of morphology-dependent behaviors, such as rheological and mechanical properties of nanocomposites or all-nanocellulose systems, such as thin films, coatings, lightweight materials, and hydrogels.

## ■ ASSOCIATED CONTENT

### SI Supporting Information

The Supporting Information is available free of charge at <https://pubs.acs.org/doi/10.1021/acsnm.1c02008>.

Detailed description of materials and methods; results of compositional analysis of untreated and pretreated feedstock; details of transmittance of nanocellulose dispersions at 600 nm; nanocellulose percolation thresholds; overview of key properties analyzed; results of water content and average film density; photographs and SEM images of untreated and pretreated feedstock; light transmittance spectra of nanocellulose dispersions; X-ray diffractograms of biomass and nanocelluloses; TEM analysis and size distribution histograms of CNCs; size distribution histograms of CNFs measured from TEM images; and photographs of self-standing TEMPO-oxidized CNF films (PDF)

## ■ AUTHOR INFORMATION

### Corresponding Author

Camila A. Rezende – Physical Chemistry Department, Institute of Chemistry, University of Campinas—UNICAMP,

Campinas, São Paulo 13083-970, Brazil; [orcid.org/0000-0002-2072-1361](https://orcid.org/0000-0002-2072-1361); Phone: +55-19-35212104; Email: [camilaiq@unicamp.br](mailto:camilaiq@unicamp.br)

### Author

Camilla H. M. Camargos – Physical Chemistry Department, Institute of Chemistry, University of Campinas—UNICAMP, Campinas, São Paulo 13083-970, Brazil; [orcid.org/0000-0002-5240-036X](https://orcid.org/0000-0002-5240-036X)

Complete contact information is available at: <https://pubs.acs.org/doi/10.1021/acsnm.1c02008>

### Funding

This work was supported by the São Paulo Research Foundation (FAPESP, grant number 2018/23769-1), National Council for Scientific and Technological Development (CNPq, grant numbers 140558/2017-9 and 420031/2018-9), and Coordenação de Aperfeiçoamento de Pessoal de Nível Superior—Brazil [CAPES, financial code 001].

### Notes

The authors declare no competing financial interest.

## ■ ACKNOWLEDGMENTS

We thank IQ-UNICAMP for providing infrastructure and access to facilities, Dr. Douglas Soares and INCT-INOMAT for AFM and TEM analyses, and Professor Edvaldo Sabadini and Fernando Bonin for rheological measurements.

## ■ REFERENCES

- (1) Abitbol, T.; Rivkin, A.; Cao, Y.; Nevo, Y.; Abraham, E.; Ben-Shalom, T.; Lapidot, S.; Shoseyov, O. Nanocellulose, a Tiny Fiber with Huge Applications. *Curr. Opin. Biotechnol.* **2016**, *39*, 76–88.
- (2) Moon, R. J.; Martini, A.; Nairn, J.; Simonsen, J.; Youngblood, J. Cellulose Nanomaterials Review: Structure, Properties and Nanocomposites. *Chem. Soc. Rev.* **2011**, *40*, 3941–3994.
- (3) Habibi, Y.; Lucia, L. a.; Rojas, O. J. Cellulose Nanocrystals: Chemistry, Self-Assembly, and Applications. *Chem. Rev.* **2010**, *110*, 3479–3500.
- (4) Isogai, A.; Saito, T.; Fukuzumi, H. TEMPO-Oxidized Cellulose Nanofibers. *Nanoscale* **2011**, *3*, 71–85.
- (5) Fortunati, E.; Puglia, D.; Monti, M.; Peponi, L.; Santulli, C.; Kenny, J. M.; Torre, L. Extraction of Cellulose Nanocrystals from Phormium Tenax Fibres. *J. Polym. Environ.* **2013**, *21*, 319–328.
- (6) Siqueira, G.; Abdillahi, H.; Bras, J.; Dufresne, A. High Reinforcing Capability Cellulose Nanocrystals Extracted from *Syngonanthus Nitens* (Capim Dourado). *Cellulose* **2010**, *17*, 289–298.
- (7) Yu, H.; Qin, Z.; Liang, B.; Liu, N.; Zhou, Z.; Chen, L. Facile Extraction of Thermally Stable Cellulose Nanocrystals with a High Yield of 93% through Hydrochloric Acid Hydrolysis under Hydrothermal Conditions. *J. Mater. Chem. A* **2013**, *1*, 3938–3944.
- (8) Sadeghifar, H.; Filpponen, I.; Clarke, S. P.; Brougham, D. F.; Argyropoulos, D. S. Production of Cellulose Nanocrystals Using Hydrobromic Acid and Click Reactions on Their Surface. *J. Mater. Sci.* **2011**, *46*, 7344–7355.
- (9) Li, B.; Xu, W.; Kronlund, D.; Määttä, A.; Liu, J.; Smått, J.-H.; Peltonen, J.; Willför, S.; Mu, X.; Xu, C. Cellulose Nanocrystals Prepared via Formic Acid Hydrolysis Followed by TEMPO-Mediated Oxidation. *Carbohydr. Polym.* **2015**, *133*, 605–612.
- (10) Camarero Espinosa, S.; Kuhnt, T.; Foster, E. J.; Weder, C. Isolation of Thermally Stable Cellulose Nanocrystals by Phosphoric Acid Hydrolysis. *Biomacromolecules* **2013**, *14*, 1223–1230.
- (11) Kassab, Z.; Syafri, E.; Tamraoui, Y.; Hannache, H.; Qaiss, A. E. K.; El Achaby, M. Characteristics of Sulfated and Carboxylated Cellulose Nanocrystals Extracted from *Juncus* Plant Stems. *Int. J. Biol. Macromol.* **2020**, *154*, 1419–1425.

- (12) Pinto, L. O.; Bernardes, J. S.; Rezende, C. A. Low-Energy Preparation of Cellulose Nanofibers from Sugarcane Bagasse by Modulating the Surface Charge Density. *Carbohydr. Polym.* **2019**, *218*, 145–153.
- (13) Zhou, Y.; Saito, T.; Bergström, L.; Isogai, A.; Bergström, L.; Isogai, A. Acid-Free Preparation of Cellulose Nanocrystals by TEMPO Oxidation and Subsequent Cavitation. *Biomacromolecules* **2018**, *19*, 633–639.
- (14) Rossi, B. R.; Pellegrini, V. O. A.; Cortez, A. A.; Chiromito, E. M. S.; Carvalho, A. J. F.; Pinto, L. O.; Rezende, C. A.; Mastelaro, V. R.; Polikarpov, I. Cellulose Nanofibers Production Using a Set of Recombinant Enzymes. *Carbohydr. Polym.* **2021**, *256*, 117510.
- (15) Wei, J.; Zhou, Y.; Lv, Y.; Wang, J.; Jia, C.; Liu, J.; Zhang, X.; Sun, J.; Shao, Z. Carboxymethyl Cellulose Nanofibrils with a Treelike Matrix: Preparation and Behavior of Pickering Emulsions Stabilization. *ACS Sustainable Chem. Eng.* **2019**, *7*, 12887–12896.
- (16) Otoni, C. G.; Figueiredo, J. S. L.; Capeletti, L. B.; Cardoso, M. B.; Bernardes, J. S.; Loh, W. Tailoring the Antimicrobial Response of Cationic Nanocellulose-Based Foams through Cryo-Templating. *ACS Appl. Bio Mater.* **2019**, *2*, 1975–1986.
- (17) Nascimento, S. A.; Scopel, E.; Rezende, C. A. Salt Crystallization Pressure as a New Method to Obtain Micro and Nanocellulose. *Cellulose* **2021**, *28*, 4069–4087.
- (18) Usov, I.; Nyström, G.; Adamcik, J.; Handschin, S.; Schütz, C.; Fall, A.; Bergström, L.; Mezzenga, R. Understanding Nanocellulose Chirality and Structure-Properties Relationship at the Single Fibril Level. *Nat. Commun.* **2015**, *6*, 1–11.
- (19) Moberg, T.; Sahlin, K.; Yao, K.; Geng, S.; Westman, G.; Zhou, Q.; Oksman, K.; Rigdahl, M. Rheological Properties of Nanocellulose Suspensions: Effects of Fibril/Particle Dimensions and Surface Characteristics. *Cellulose* **2017**, *24*, 2499–2510.
- (20) Fukuzumi, H.; Saito, T.; Isogai, A. Influence of TEMPO-Oxidized Cellulose Nanofibril Length on Film Properties. *Carbohydr. Polym.* **2013**, *93*, 172–177.
- (21) Kalashnikova, I.; Bizot, H.; Cathala, B.; Capron, I. Modulation of Cellulose Nanocrystals Amphiphilic Properties to Stabilize Oil/Water Interface. *Biomacromolecules* **2012**, *13*, 267–275.
- (22) Guo, S.; Li, X.; Kuang, Y.; Liao, J.; Liu, K.; Li, J.; Mo, L.; He, S.; Zhu, W.; Song, J.; Song, T.; Rojas, O. J. Residual Lignin in Cellulose Nanofibrils Enhances the Interfacial Stabilization of Pickering Emulsions. *Carbohydr. Polym.* **2021**, *253*, 117223.
- (23) Liu, C.; Li, M.-C.; Chen, W.; Huang, R.; Hong, S.; Wu, Q.; Mei, C. Production of Lignin-Containing Cellulose Nanofibers Using Deep Eutectic Solvents for UV-Absorbing Polymer Reinforcement. *Carbohydr. Polym.* **2020**, *246*, 116548.
- (24) Espinosa, E.; Bascón-Villegas, I.; Rosal, A.; Pérez-Rodríguez, F.; Chinga-Carrasco, G.; Rodríguez, A. PVA/(Ligno)Nanocellulose Biocomposite Films. Effect of Residual Lignin Content on Structural, Mechanical, Barrier and Antioxidant Properties. *Int. J. Biol. Macromol.* **2019**, *141*, 197–206.
- (25) Yuan, T.; Zeng, J.; Wang, B.; Cheng, Z.; Chen, K. Lignin Containing Cellulose Nanofibers (LCNFs): Lignin Content-Morphology-Rheology Relationships. *Carbohydr. Polym.* **2021**, *254*, 117441.
- (26) Iglesias, M. C.; Shiviyari, N.; Norris, A.; Martin-Sampedro, R.; Eugenio, M. E.; Lahtinen, P.; Auad, M. L.; Elder, T.; Jiang, Z.; Frazier, C. E.; Peresin, M. S. The Effect of Residual Lignin on the Rheological Properties of Cellulose Nanofibril Suspensions. *J. Wood Chem. Technol.* **2020**, *40*, 370–381.
- (27) Scopel, E.; Rezende, C. A. Biorefinery On-Demand: Modulating Pretreatments to Recover Lignin, Hemicellulose, and Extracts as Co-Products during Ethanol Production. *Ind. Crops Prod.* **2021**, *163*, 113336.
- (28) Camargos, C. H. M.; Figueiredo, J. C. D.; Pereira, F. V. Cellulose Nanocrystal-Based Composite for Restoration of Lacunae on Damaged Documents and Artworks on Paper. *J. Cult. Herit.* **2017**, *23*, 170–175.
- (29) Fukuzumi, H.; Saito, T.; Iwata, T.; Kumamoto, Y.; Isogai, A. Transparent and High Gas Barrier Films of Cellulose Nanofibers Prepared by TEMPO-Mediated Oxidation. *Biomacromolecules* **2009**, *10*, 162–165.
- (30) Li, F.; Biagioni, P.; Bollani, M.; Maccagnan, A.; Piergiovanni, L. Multi-Functional Coating of Cellulose Nanocrystals for Flexible Packaging Applications. *Cellulose* **2013**, *20*, 2491–2504.
- (31) Ferreira, E. S.; Rezende, C. A.; Cranston, E. D. Fundamentals of Cellulose Lightweight Materials: Bio-Based Assemblies with Tailored Properties. *Green Chem.* **2021**, *23*, 3542.
- (32) Nascimento, S. A.; Rezende, C. A. Combined Approaches to Obtain Cellulose Nanocrystals, Nanofibrils and Fermentable Sugars from Elephant Grass. *Carbohydr. Polym.* **2018**, *180*, 38–45.
- (33) Rezende, C. A.; Atta, B. W.; Breitzkreitz, M. C.; Simister, R.; Gomez, L. D.; McQueen-Mason, S. J. Optimization of Biomass Pretreatments Using Fractional Factorial Experimental Design. *Biotechnol. Biofuels* **2018**, *11*, 206.
- (34) Sluiter, J. B.; Ruiz, R. O.; Scarlata, C. J.; Sluiter, A. D.; Templeton, D. W. Compositional Analysis of Lignocellulosic Feedstocks. 1. Review and Description of Methods. *J. Agric. Food Chem.* **2010**, *58*, 9043–9053.
- (35) Jackson, J. C.; Camargos, C. H. M.; Noronha, V. T.; Paula, A. J.; Rezende, C. A.; Faria, A. F. Sustainable Cellulose Nanocrystals for Improved Antimicrobial Properties of Thin Film Composite Membranes. *ACS Sustainable Chem. Eng.* **2021**, *9*, 6534–6540.
- (36) Segal, L.; Creely, J. J.; Martin, A. E.; Conrad, C. M. An Empirical Method for Estimating the Degree of Crystallinity of Native Cellulose Using the X-Ray Diffractometer. *Text. Res. J.* **1959**, *29*, 786–794.
- (37) Shinoda, R.; Saito, T.; Okita, Y.; Isogai, A. Relationship between Length and Degree of Polymerization of TEMPO-Oxidized Cellulose Nanofibrils. *Biomacromolecules* **2012**, *13*, 842–849.
- (38) Henriksson, M.; Berglund, L. A.; Isaksson, P.; Lindström, T.; Nishino, T. Cellulose Nanopaper Structures of High Toughness. *Biomacromolecules* **2008**, *9*, 1579–1585.
- (39) Beck, S.; Méthot, M.; Bouchard, J. General Procedure for Determining Cellulose Nanocrystal Sulfate Half-Ester Content by Conductometric Titration. *Cellulose* **2015**, *22*, 101–116.
- (40) Lin, N.; Bruzzese, C.; Dufresne, A. TEMPO-Oxidized Nanocellulose Participating as Crosslinking Aid for Alginate-Based Sponges. *ACS Appl. Mater. Interfaces* **2012**, *4*, 4948–4959.
- (41) Abitbol, T.; Kloser, E.; Gray, D. G. Estimation of the Surface Sulfur Content of Cellulose Nanocrystals Prepared by Sulfuric Acid Hydrolysis. *Cellulose* **2013**, *20*, 785–794.
- (42) Petridis, L.; Smith, J. C. Molecular-Level Driving Forces in Lignocellulosic Biomass Deconstruction for Bioenergy. *Nat. Rev. Chem.* **2018**, *2*, 382–389.
- (43) Montanari, S.; Roumani, M.; Heux, L.; Vignon, M. R. Topochemistry of Carboxylated Cellulose Nanocrystals Resulting from TEMPO-Mediated Oxidation. *Macromolecules* **2005**, *38*, 1665–1671.
- (44) Trache, D.; Tarchoun, A. F.; Derradji, M.; Hamidon, T. S.; Masruchin, N.; Brosse, N.; Hussin, M. H. Nanocellulose: From Fundamentals to Advanced Applications. *Front. Chem.* **2020**, *8*, 392.
- (45) Dunlop, M. J.; Clemons, C.; Reiner, R.; Sabo, R.; Agarwal, U. P.; Bissessur, R.; Sojoudiasli, H.; Carreau, P. J.; Acharya, B. Towards the Scalable Isolation of Cellulose Nanocrystals from Tunicates. *Sci. Rep.* **2020**, *10*, 1–13.
- (46) Solala, I.; Iglesias, M. C.; Peresin, M. S. On the Potential of Lignin-Containing Cellulose Nanofibrils (LCNFs): A Review on Properties and Applications. *Cellulose* **2020**, *27*, 1853–1877.
- (47) Tarrés, Q.; Ehman, N. V.; Vallejos, M. E.; Area, M. C.; Delgado-Aguilar, M.; Mutjé, P. Lignocellulosic Nanofibers from Triticale Straw: The Influence of Hemicelluloses and Lignin in Their Production and Properties. *Carbohydr. Polym.* **2017**, *163*, 20–27.
- (48) Daicho, K.; Kobayashi, K.; Fujisawa, S.; Saito, T. Crystallinity-Independent yet Modification-Dependent True Density of Nanocellulose. *Biomacromolecules* **2020**, *21*, 939–945.
- (49) Daicho, K.; Saito, T.; Fujisawa, S.; Isogai, A. The Crystallinity of Nanocellulose: Dispersion-Induced Disordering of the Grain

Boundary in Biologically Structured Cellulose. *ACS Appl. Nano Mater.* **2018**, *1*, 5774–5785.

(50) Qu, R.; Tang, M.; Wang, Y.; Li, D.; Wang, L. TEMPO-Oxidized Cellulose Fibers from Wheat Straw: Effect of Ultrasonic Pretreatment and Concentration on Structure and Rheological Properties of Suspensions. *Carbohydr. Polym.* **2021**, *255*, 117386.

(51) Chen, W.; Yu, H.; Liu, Y.; Hai, Y.; Zhang, M.; Chen, P. Isolation and Characterization of Cellulose Nanofibers from Four Plant Cellulose Fibers Using a Chemical-Ultrasonic Process. *Cellulose* **2011**, *18*, 433–442.

(52) Okita, Y.; Saito, T.; Isogai, A. TEMPO-Mediated Oxidation of Softwood Thermomechanical Pulp. *Holzforschung* **2009**, *63*, 529–535.

(53) Fan, J.-s.; Li, Y.-h. Maximizing the Yield of Nanocrystalline Cellulose from Cotton Pulp Fiber. *Carbohydr. Polym.* **2012**, *88*, 1184–1188.

(54) Luzi, F.; Puglia, D.; Sarasini, F.; Tirillò, J.; Maffei, G.; Zuorro, A.; Lavecchia, R.; Kenny, J. M.; Torre, L. Valorization and Extraction of Cellulose Nanocrystals from North African Grass: *Ampelodesmos Mauritanicus* (Diss). *Carbohydr. Polym.* **2019**, *209*, 328–337.

(55) Isogai, T.; Saito, T.; Isogai, A. Wood Cellulose Nanofibers Prepared by TEMPO Electro-Mediated Oxidation. *Cellulose* **2011**, *18*, 421–431.

(56) Chen, L.; Wang, Q.; Hirth, K.; Baez, C.; Agarwal, U. P.; Zhu, J. Y. Tailoring the Yield and Characteristics of Wood Cellulose Nanocrystals (CNC) Using Concentrated Acid Hydrolysis. *Cellulose* **2015**, *22*, 1753–1762.

(57) Rohaizu, R.; Wanrosli, W. D. Sono-Assisted TEMPO Oxidation of Oil Palm Lignocellulosic Biomass for Isolation of Nanocrystalline Cellulose. *Ultrason. Sonochem.* **2017**, *34*, 631–639.

(58) Ding, S.-Y.; Himmel, M. E. The Maize Primary Cell Wall Microfibril: A New Model Derived from Direct Visualization. *J. Agric. Food Chem.* **2006**, *54*, 597.

(59) Buxton, D. R.; Redfean, D. D. Plant Limitations to Fiber Digestion and Utilization. *J. Nutr.* **1997**, *127*, 814S–818S.

(60) Brown, R. M. Cellulose Structure and Biosynthesis: What Is in Store for the 21st Century? *J. Polym. Sci., Part A: Polym. Chem.* **2004**, *42*, 487–495.

(61) Battista, O. A.; Coppick, S.; Howsmon, J. A.; Morehead, F. F.; Sisson, W. A. Level-Off Degree of Polymerization. *Ind. Eng. Chem.* **1956**, *48*, 333–335.

(62) Foster, E. J.; Moon, R. J.; Agarwal, U. P.; Bortner, M. J.; Bras, J.; Camarero-Espinosa, S.; Chan, K. J.; Clift, M. J. D.; Cranston, E. D.; Eichhorn, S. J.; Fox, D. M.; Hamad, W. Y.; Heux, L.; Jean, B.; Korey, M.; Nieh, W.; Ong, K. J.; Reid, M. S.; Renneckar, S.; Roberts, R.; Shatkin, J. A.; Simonsen, J.; Stinson-Bagby, K.; Wanasekara, N.; Youngblood, J. Current Characterization Methods for Cellulose Nanomaterials. *Chem. Soc. Rev.* **2018**, *47*, 2609–2679.

(63) Fukuzumi, H.; Saito, T.; Okita, Y.; Isogai, A. Thermal Stabilization of TEMPO-Oxidized Cellulose. *Polym. Degrad. Stab.* **2010**, *95*, 1502–1508.

(64) Klemm, D.; Kramer, F.; Moritz, S.; Lindström, T.; Ankerfors, M.; Gray, D.; Dorris, A. Nanocelluloses: A New Family of Nature-Based Materials. *Angew. Chem., Int. Ed.* **2011**, *50*, 5438–5466.

(65) Qi, W.; Yu, J.; Zhang, Z.; Xu, H.-N. Effect of PH on the Aggregation Behavior of Cellulose Nanocrystals in Aqueous Medium. *Mater. Res. Express* **2019**, *6*, 125078.

(66) Nechyporchuk, O.; Belgacem, M. N.; Pignon, F. Current Progress in Rheology of Cellulose Nanofibril Suspensions. *Biomacromolecules* **2016**, *17*, 2311–2320.

(67) Liao, J.; Pham, K. A.; Breedveld, V. Rheological Characterization and Modeling of Cellulose Nanocrystal and TEMPO-Oxidized Cellulose Nanofibril Suspensions. *Cellulose* **2020**, *27*, 3741–3757.

(68) Wakabayashi, M.; Fujisawa, S.; Saito, T.; Isogai, A. Nanocellulose Film Properties Tunable by Controlling Degree of Fibrillation of TEMPO-Oxidized Cellulose. *Front. Chem.* **2020**, *8*, 37.

(69) Saito, T.; Hirota, M.; Tamura, N.; Kimura, S.; Fukuzumi, H.; Heux, L.; Isogai, A. Individualization of Nano-Sized Plant Cellulose

Fibrils by Direct Surface Carboxylation Using TEMPO Catalyst under Neutral Conditions. *Biomacromolecules* **2009**, *10*, 1992–1996.